Special Issue Article

Advances in Mechanical Engineering

Advances in Mechanical Engineering
2017, Vol. 9(7) 1–13

DOI: 10.1177/1687814017707649
journals.sagepub.com/home/ade
SAGE

Identifying the stiffness parameters of a structure using a subspace approach and the Gram–Schmidt process in a wavelet domain

Wei-Chih Su[1], Chiung-Shiann Huang[2], Ho-Cheng Lien[1] and Quang-Tuyen Le[2]

Abstract

This article presents a procedure to improve the accuracy of calculated stiffness matrix of a structure based on the identified modal parameters from its measured responses. First, a continuous wavelet transform is applied to the measured responses of a structure, and the state–space model can be reconstructed by the wavelet coefficients of acceleration that can be obtained from the measured noisy responses. The modal parameters are identified using the subspace approach. Second, the identified mode shapes are corrected via Gram–Schmidt process. Finally, the identified natural frequencies and the corrected mode shapes in previous steps are utilized to build the stiffness matrix of structure. The accuracy of the proposed approach is numerically confirmed, and the noise effects on the ability to precisely identify the stiffness matrix are also investigated. The measured data of two eight-story steel frames in a shaking table test are analyzed to demonstrate the applicability of the procedure to real structures.

Keywords

Damage assessment, subspace approach, Gram–Schmidt process, modal identification, wavelet transform

Date received: 14 June 2016; accepted: 6 April 2017

Academic Editor: Stephen D Prior

Introduction

Damage to a structure is caused by many sources, especially intense loading during a strong earthquake and the degradation of structural material. Identifying the location and level of structural damage is critical to the investigation of the serviceability and safety of structures. Early evaluation of damage or structural degradation is essential for preventing disastrous accidents. Studies on structural health monitoring have been receiving increasing attentions in the field of civil engineering.

The modal parameters of a structure can be used to figure out the stiffness characteristics of a structure. For this reason, the damaged structures can be detected by the change of the modal parameters. In recent decades, the modal identification methods that are implemented in time domain, frequency domain, or time–frequency domain are simple and extensively adopted.[1–3] Various formulations in time–frequency domain are performed to process the noisy data from various field tests.[4,5] The proposed procedure is a

[1]National Center for High-Performance Computing, National Applied Research Laboratories, Hsinchu, Taiwan
[2]Department of Civil Engineering, National Chiao Tung University, Hsinchu, Taiwan

Corresponding author:
Wei-Chih Su, National Center for High-Performance Computing, National Applied Research Laboratories, No. 7, R&D 6th Rd., Hsinchu Science Park, Hsinchu 30076, Taiwan.
Email: wichcv86@gmail.com

typical example of the cooperation between a state–space model and a subspace approach[6,7] in time–frequency domain for the modal identification. However, the accuracy of the identified modal parameters is always reduced by the imperfections of the measured responses, which usually comprise certain noise from unknown input or system resolutions.

Due to the strong capability of data de-noising, continuous wavelet transforms have been discussed in some studies that aim to identify the modal parameters of a linear system.[8–10] Huang and Su[11] utilized continuous wavelet transform for the earthquake responses of a structure using various wavelet functions. They proposed modal identification procedures that are based on a time series model to determine structural modal parameters of the system using the coefficient of a wavelet transform.

As mentioned previously, the identified modal parameters could be used to observe whether the structure is damaged or not. But, the damaged location is difficult to be found from the results of modal identification. A stiffness matrix–based approach[7,12] that employs identified modal parameters and given mass properties is a vibration-based damage detection approach for finding the damaged location. The stiffness parameters have been identified for controlling the flexible members in robotic manipulator or marine riser system.[13–15] In the ideal experimental condition, the clear and noise-free responses would be measured. However, the noisy vibration is always obtained in the on-site test; for this reason, the de-noising procedure needs to apply on the modal identification process.

Despite the de-noising procedure reducing the influence of noise in the frequency identification, it often removes certain parts' signal energy and causes identification error for mode shapes in higher modes. The orthogonality property, which cooperates with the mass and stiffness matrices of the mode shapes, can be used to correct the identified mode shapes. In linear algebra, many orthogonalization algorithms and approaches have been proposed and widely used for computing an orthogonal basis, such as Householder transformations, Givens rotations, and Gram–Schmidt process.[16] There are two basic computational variants for executing the Gram–Schmidt process: the classical Gram–Schmidt algorithm and the modified Gram–Schmidt algorithm.[17] For the rounding error, the classical Gram–Schmidt algorithm may produce a set of vectors which is lost orthogonality.[18] The modified Gram–Schmidt algorithm has better numerical properties stable than the classical Gram–Schmidt algorithm.[19]

This study proposes a comprehensive procedure to accurately obtain a stiffness matrix using the identified modal parameters based on Gram–Schmidt process. The identified modal parameters are calculated from a subspace approach in Morlet wavelet domain. The identified mode shapes are corrected by applying the given mass properties and Gram–Schmidt process. The structural stiffness parameters can be calculated via the previous identified natural frequencies and the corrected mode shapes. The applicability of this approach was verified in a numerical analysis using simulated earthquake acceleration responses of a six-story shear building. The measured noisy responses and input with 10% variance of the noise-to-signal ratio (NSR) are processed. The proposed procedure was successfully applied to the measured acceleration responses of two eight-story steel frames in a shaking table test and proved the feasibility of this procedure in practical cases. The columns in the first and third story of the steel frame were constructed of steel plates with cutoff.

Methodology

Subspace approach in Morlet wavelet domain

In the case of a linear structure, the equation of motion for the dynamic responses can be expressed as follows

$$\mathbf{M}\ddot{\mathbf{x}} + \mathbf{C}\dot{\mathbf{x}} + \mathbf{K}\mathbf{x} = \mathbf{f} \tag{1}$$

where $\mathbf{M}$, $\mathbf{C}$, and $\mathbf{K}$ represent the mass matrix, damping matrix, and stiffness matrices, respectively, of the system; $\ddot{\mathbf{x}}$ is the measured acceleration response vector; $\dot{\mathbf{x}}$ is the measured velocity response vector; $\mathbf{x}$ is the displacement response vectors; and $\mathbf{f}$ represents for the input force vectors. Consider that the observed degrees of freedoms apply to the case of incomplete observation and only acceleration or velocity responses are measured. Here, the expression $\mathbf{y} = \mathbf{L}\mathbf{x}$ is used to describe the observed responses, in which $\mathbf{L}$ is a matrix with components equal to 0 or 1 according to the non-observed or observed conditions.

The state–space model is generally considered in the following formulation

$$\begin{cases} \mathbf{z}_{k+1} = \mathbf{A}\mathbf{z}_k + \mathbf{B}\mathbf{f}_k \\ \mathbf{y}_k = \mathbf{E}\mathbf{z}_k + \mathbf{D}\mathbf{f}_k \end{cases} \tag{2}$$

where $\mathbf{A}$, $\mathbf{B}$, $\mathbf{E}$, and $\mathbf{D}$ are the system matrices that are related to $\mathbf{M}$, $\mathbf{C}$, and $\mathbf{K}$; $\mathbf{z} = \begin{bmatrix} \mathbf{x}^{\mathbf{T}} & \dot{\mathbf{x}}^{\mathbf{T}} \end{bmatrix}^{\mathbf{T}}$ is a state variable. As shown in equation (2), the following recursive formula can be obtained

$$\mathbf{y}_{k+s} = \mathbf{E}\mathbf{A}^s\mathbf{z}_k + \mathbf{D}\mathbf{f}_{k+s} + \sum_{i=1}^{s} \mathbf{E}\mathbf{A}^{i-1}\mathbf{B}\mathbf{f}_{k+s+i-1} \tag{3}$$

Applying the continuous Morlet wavelet transform to equation (3) and treating $\mathbf{y}$ and $\mathbf{f}$ as vector functions yield the following

$$\mathscr{W}_{\psi_\sigma}\mathbf{y}_{k+s} = \mathbf{E}\mathbf{A}^{s}\mathscr{W}_{\psi_\sigma}\mathbf{z}_k + \mathbf{D}\mathscr{W}_{\psi_\sigma}\mathbf{f}_{k+s} + \sum_{i=1}^{s}\mathbf{E}\mathbf{A}^{i-1}\mathbf{B}\mathscr{W}_{\psi_\sigma}\mathbf{f}_{k+s+i-1} \tag{4}$$

where the definition of the continuous wavelet transform for a function $f(t)$ can be written as follows

$$\mathscr{W}_{\psi_\sigma}f(p,a) = \frac{1}{\sqrt{a}}\int_{-\infty}^{+\infty} f(t)\psi_\sigma^*\left(\frac{t-p}{a}\right) \tag{5}$$

Variable a is the dilation of the scale parameter, variable p is the translation parameter, and $\psi_\sigma(t)$ is the mother function. The superscript * denotes the complex conjugate. Morlet wavelets are utilized to form equation (5). Equation (6) is used to define the standard Morlet mother wavelet with order σ

$$\psi_\sigma(t) = u_\sigma \pi^{-1/4} e^{-t^2/2}\left(e^{i\sigma t} - e^{-\sigma^2/2}\right) \tag{6}$$

where $u_\sigma = (1 + e^{-\sigma^2} - 2e^{-3\sigma^2/4})^{-1/2}$ is the normalization constant. Using equation (4), one can further construct the following

$$\mathscr{W}_{\psi_\sigma}\mathbf{y}_{k,s} = \Theta_\alpha \mathscr{W}_{\psi_\sigma}\mathbf{z}_k + \mathbf{\Phi}_\alpha \mathscr{W}_{\psi_\sigma}\mathbf{f}_{k,s} \tag{7}$$

where

$$\begin{aligned}
&\mathscr{W}_{\psi_\sigma}\mathbf{y}_{k,s} = \left[\mathscr{W}_{\psi_\sigma}\mathbf{y}_k^{\mathbf{T}} \quad \mathscr{W}_{\psi_\sigma}\mathbf{y}_{k+1}^{\mathbf{T}} \quad \cdots \quad \mathscr{W}_{\psi_\sigma}\mathbf{y}_{k+s-1}^{\mathbf{T}}\right]^{\mathbf{T}}\\
&\Theta_\alpha = \left[\mathbf{E}^{\mathbf{T}} \quad (\mathbf{E}\mathbf{A})^{\mathbf{T}} \quad \cdots \quad \left(\mathbf{E}\mathbf{A}^{s-1}\right)^{\mathbf{T}}\right]^{\mathbf{T}}\\
&\mathbf{\Phi}_\alpha = \begin{bmatrix} \mathbf{D} & 0 & 0 & \cdots & 0\\ \mathbf{E}\mathbf{B} & \mathbf{D} & 0 & \cdots & 0\\ \mathbf{E}\mathbf{A}\mathbf{B} & \mathbf{E}\mathbf{B} & \mathbf{D} & \cdots & 0\\ \vdots & & & & \\ \mathbf{E}\mathbf{A}^{s-1}\mathbf{B} & \mathbf{E}\mathbf{A}^{s-2}\mathbf{B} & \cdots & & \mathbf{D}\end{bmatrix}\\
&\mathscr{W}_{\psi_\sigma}\mathbf{f}_{k,s} = \left[\mathscr{W}_{\psi_\sigma}\mathbf{f}_k^{\mathbf{T}} \quad \mathscr{W}_{\psi_\sigma}\mathbf{f}_{k+1}^{\mathbf{T}} \quad \cdots \quad \mathscr{W}_{\psi_\sigma}\mathbf{f}_{k+s-1}^{\mathbf{T}}\right]^{\mathbf{T}}
\end{aligned} \tag{8}$$

where the two sets $\mathscr{W}_{\psi_\sigma}\mathbf{y}_{k,s}$ and $\mathscr{W}_{\psi_\sigma}\mathbf{y}_{k,s}$ are the coefficients of Morlet wavelet transform of $\mathbf{y}_k$ and $\mathbf{f}_k$, respectively. Equation (7) can be re-written as follows

$$\hat{\mathbf{Y}}_N = \Theta_\alpha \hat{\mathbf{Z}}_N + \mathbf{\Phi}_\alpha \hat{\mathbf{F}}_N \tag{9}$$

where

$$\begin{cases}
\hat{\mathbf{Y}}_{k,N} = \left[\mathscr{W}_{\psi_\sigma}\mathbf{y}_{k,s} \quad \mathscr{W}_{\psi_\sigma}\mathbf{y}_{k+1,s} \quad \cdots \quad \mathscr{W}_{\psi_\sigma}\mathbf{y}_{k+N-1,s}\right]\\
\hat{\mathbf{Z}}_{k,N} = \left[\mathscr{W}_{\psi_\sigma}\mathbf{z}_k \quad \mathscr{W}_{\psi_\sigma}\mathbf{z}_{k+1} \quad \cdots \quad \mathscr{W}_{\psi_\sigma}\mathbf{z}_{k+N-1}\right]\\
\hat{\mathbf{F}}_{k,N} = \left[\mathscr{W}_{\psi_\sigma}\mathbf{f}_{k,s} \quad \mathscr{W}_{\psi_\sigma}\mathbf{f}_{k+1,s} \quad \cdots \quad \mathscr{W}_{\psi_\sigma}\mathbf{f}_{k+N-1,s}\right]
\end{cases} \tag{10}$$

A brief summary of the subspace approach procedure, which was organized by Huang et al.[7] and in more detail by Huang and Lin,[6] is described as follows

1. Define an orthogonal projection matrix $\prod_f^{\perp} = \mathbf{I} - \hat{\mathbf{F}}_{k,N}^{\mathbf{T}}(\hat{\mathbf{F}}_{k,N}\hat{\mathbf{F}}_{k,N}^{\mathbf{T}})^{-1}\hat{\mathbf{F}}_{k,N}$ onto the null space of $\hat{\mathbf{F}}_{k,N}$;
2. Introduce the instrumental variables $\mathbf{P} = [\hat{\mathbf{F}}_{p,N}^{\mathbf{T}} \quad \hat{\mathbf{Y}}_{p,N}^{\mathbf{T}}]^{\mathbf{T}}$;
3. Calculate the weighting matrices $\mathbf{W}_r = \mathbf{I}$ and $\mathbf{W}_c = (\mathbf{P}\Pi_f^{\perp}\mathbf{P}^{\mathbf{T}}/N)^{-1/2}$;
4. Define the matrix $\bar{\mathbf{H}} = \mathbf{W}_r\hat{\mathbf{Y}}_{k,N}\prod_f^{\perp}\mathbf{P}\mathbf{W}_c/N$;
5. Apply singular value decomposition on $\bar{\mathbf{H}} \cong \mathbf{Q}_{\bar{n}}\mathbf{D}_{\bar{n}}\mathbf{V}_{\bar{n}}^{\mathbf{T}}$;
6. Let $\mathbf{\Gamma}_\alpha = \bar{\mathbf{\Gamma}}_\alpha\mathbf{T}_{\bar{n}}$, where $\bar{\mathbf{\Gamma}}_\alpha = \mathbf{W}_r^{-1}\mathbf{Q}_{\bar{n}}\mathbf{D}_{\bar{n}}^{-1/2}$; $\mathbf{T}_{\bar{n}} = \mathbf{D}_{\bar{n}}^{-1/2}\mathbf{V}_{\bar{n}}\,(\hat{\mathbf{Z}}_{k,N}\prod_f^{\perp}\mathbf{P}\mathbf{W}_c/N)^{-1/2}$;
7. Rewrite equation (7) as $\mathscr{W}_{\psi_\sigma}\mathbf{y}_{k,s} = \bar{\mathbf{\Gamma}}_\alpha\bar{\mathbf{z}}_k + \mathbf{\Phi}_\alpha\mathscr{W}_{\psi_\sigma}\mathbf{f}_{k,s}$, where $\bar{\mathbf{z}}_k = \mathbf{T}_{\bar{n}}\mathscr{W}_{\psi_\sigma}\mathbf{z}_k$;
8. $\bar{\mathbf{\Gamma}}_\alpha$ can be established by $\bar{\mathbf{\Gamma}}_\alpha = \left[\bar{\mathbf{E}}^{\mathbf{T}} \quad (\bar{\mathbf{E}}\bar{\mathbf{A}})^{\mathbf{T}} \quad \cdots \quad (\bar{\mathbf{E}}\bar{\mathbf{A}}^{s-1})^{\mathbf{T}}\right]^{\mathbf{T}}$;
9. Define $\bar{\mathbf{\Gamma}}_{\alpha 1} = [\bar{\mathbf{E}}^{\mathbf{T}} \quad (\bar{\mathbf{E}}\bar{\mathbf{A}})^{\mathbf{T}} \quad \cdots \quad (\bar{\mathbf{E}}\bar{\mathbf{A}}^{s-2})^{\mathbf{T}}]^{\mathbf{T}}$ and $\bar{\mathbf{\Gamma}}_{\alpha 2} = [(\bar{\mathbf{E}}\bar{\mathbf{A}})^{\mathbf{T}} \quad (\bar{\mathbf{E}}\bar{\mathbf{A}}^2)^{\mathbf{T}} \quad \cdots \quad (\bar{\mathbf{E}}\bar{\mathbf{A}}^{s-1})^{\mathbf{T}}]^{\mathbf{T}}$;
10. Calculate $\bar{\mathbf{A}}$ by solving the linear equation $\bar{\mathbf{\Gamma}}_{\alpha 2} = \bar{\mathbf{\Gamma}}_{\alpha 1}\bar{\mathbf{A}}$.

Identification of modal parameters

The modal parameters of a system are generally identified using the eigenvalues and eigenvectors of the system matrix $\mathbf{A}$ in equation (2). The terms of the space–state variable are used to express the equation of motion. However, matrix $\mathbf{A}$ cannot be directly determined from the preceding derivation. To identify the modal parameters of a structure, employ matrix $\bar{\mathbf{A}}$, which is characterized as follows

$$\bar{\lambda}_j = e^{\lambda_j \Delta t}; \quad \bar{\boldsymbol{\varphi}}_j = \mathbf{T}_{\bar{n}}\boldsymbol{\varphi}_j \tag{11}$$

where λ_j and $\boldsymbol{\varphi}_j$ are the jth eigenvalue of $\mathbf{A}$ and the jth eigenvector of $\mathbf{A}$, respectively, and $\bar{\lambda}_j$ and $\bar{\boldsymbol{\varphi}}_j$ are the jth eigenvalue of $\bar{\mathbf{A}}$ and the jth eigenvector of $\bar{\mathbf{A}}$, respectively. In equation (11), $\boldsymbol{\varphi}_j$ cannot be estimated because $\mathbf{T}_{\bar{n}}$ is unknown. To overcome this challenge, the modal shape $\boldsymbol{\varphi}_{j,y}$, which corresponds to the observed degrees of freedom, needs to be determined first.

Based on the scheme in section "Subspace approach in Morlet wavelet domain," a new relationship can be determined

$$\boldsymbol{\varphi}_{j,y} = \bar{\mathbf{E}}\bar{\boldsymbol{\varphi}}_j \tag{12}$$

The eigenvalues of $\mathbf{A}$ and $\bar{\mathbf{A}}$ are complex numbers and can be expressed as follows

$$\begin{aligned}\lambda_j &= \alpha_j + i\beta_j \\ \bar{\lambda}_j &= a_j + ib_j\end{aligned} \tag{13}$$

From the relationship between the eigenvalues of $\mathbf{A}$ and $\bar{\mathbf{A}}$ in equation (11), one has

$$\begin{aligned}\alpha_j &= \frac{\ln\left(a_j^2 + b_j^2\right)}{2\Delta t} \\ \beta_j &= \frac{an^{-1}\left(b_j/a_j\right)}{t/\Delta t}\end{aligned} \tag{14}$$

The modal parameters of the structural system can be determined as follows

$$\begin{aligned}\omega_j &= \sqrt{\alpha_j^2 + \beta_j^2} \\ \xi_j &= \frac{-\alpha_j}{\omega_j}\end{aligned} \tag{15}$$

where ω_j is the jth pseudo-undamped circular natural frequency, and ξ_j is the jth modal damping ratio of the structural system.

Construction of stiffness matrix

Consider the equation of motion of a structural dynamic response, as shown in equation (1), and assume the damping properties in structure, the modal mode shapes perform the orthogonality property with the mass and stiffness matrix[20] as follows

$$\mathbf{M}_D = \boldsymbol{\varphi}^{\mathrm{T}}\mathbf{M}\boldsymbol{\varphi}; \quad \mathbf{K}_D = \boldsymbol{\varphi}^{\mathrm{T}}\mathbf{K}\boldsymbol{\varphi} \tag{16}$$

where $\mathbf{M}_D$ is the diagonal modal mass matrix, and $\mathbf{K}_D$ is the diagonal modal stiffness matrix of the structure. The square of the modal frequencies is described as an equation of matrix $\boldsymbol{\Lambda}$ as follows

$$\boldsymbol{\Lambda} = \mathbf{M}_D^{-\mathbf{T}/2}\mathbf{K}_D\mathbf{M}_D^{-1/2} = \mathbf{M}_D^{-\mathbf{T}/2}\boldsymbol{\varphi}^{\mathbf{T}}\mathbf{K}\boldsymbol{\varphi}\mathbf{M}_D^{-1/2} \tag{17}$$

Assuming that the mass matrix was given, the stiffness matrix can be obtained as follows

$$\mathbf{K} = \boldsymbol{\varphi}^{-\mathbf{T}}\mathbf{M}_D^{\mathbf{T}/2}\boldsymbol{\Lambda}\mathbf{M}_D^{1/2}\boldsymbol{\varphi}^{-1} \tag{18}$$

However, the error in the identified higher modal is larger than the errors in other identified modals because the de-noising procedure removes certain parts' signal energy. For this reason, a correction procedure of identified mode shapes based on the Gram–Schmidt process is proposed. First, one can obtain the identical equation as follows

$$\bar{\boldsymbol{\varphi}}^{\mathbf{T}}\bar{\boldsymbol{\varphi}} = \mathbf{I} \tag{19}$$

where

$$\bar{\boldsymbol{\varphi}} = \mathbf{M}^{1/2}\boldsymbol{\varphi}\mathbf{M}_D^{-1/2} \tag{20}$$

As shown in equation (12), $\bar{\boldsymbol{\varphi}}$ is a unitary matrix. The column vectors of $\bar{\boldsymbol{\varphi}}$ are implied to be an orthogonal set. However, the $\hat{\boldsymbol{\varphi}}$ constructed by the identified mode shapes during the de-noising procedure is not a unitary matrix. In this situation, the column vectors of $\hat{\boldsymbol{\varphi}}$ comprise a linear independent set.

Gram–Schmidt orthogonalization, which is also referred to as the Gram–Schmidt process, is a procedure that takes a nonorthogonal set of linearly independent functions and constructs an orthogonal basis over an arbitrary interval with respect to an arbitrary weighting function. The complete procedure is described as follows:

1. Define the projection operator

$$P_{\tilde{\boldsymbol{\varphi}}_i}\left(\hat{\boldsymbol{\varphi}}_j\right) = \frac{\tilde{\boldsymbol{\varphi}}_i^{\mathbf{T}}\hat{\boldsymbol{\varphi}}_j}{\tilde{\boldsymbol{\varphi}}_i^{\mathbf{T}}\tilde{\boldsymbol{\varphi}}_i}\tilde{\boldsymbol{\varphi}}_i \tag{21}$$

2. Calculate orthogonal vectors

$$\tilde{\boldsymbol{\varphi}}_i = \hat{\boldsymbol{\varphi}}_i - \sum_{j=1}^{i-1} P_{\tilde{\boldsymbol{\varphi}}_j}\left(\hat{\boldsymbol{\varphi}}_i\right) \tag{22}$$

3. Normalize the orthogonal vectors $\tilde{\boldsymbol{\varphi}}_i$

$$\bar{\boldsymbol{\varphi}}_i = \frac{\tilde{\boldsymbol{\varphi}}_i}{\|\tilde{\boldsymbol{\varphi}}_i\|} \tag{23}$$

Based on the given mass properties, the Gram–Schmidt process is applied to the identified model shapes. The identified higher modal is corrected, and the stiffness matrix can be constructed.

Numerical verification

To prove that the proposed procedure is sensitive and realizable in the numerical analysis, a six-story shear building (Figure 1), which is simulated by Runge–Kutta method, was subjected to the 1999 Chi-Chi earthquake at the base. The modal damping ratio is set to constant value of 5% in the simulation process. Table 1 lists the theoretical modal parameters of the six-story frame. Figure 1 describes the acceleration responses of the shear building and the input excitation at $t = 5$–45 s with $\Delta t = 0.005$ s, which were employed in the identification process. The frequency response function, which is well-known modal identification approach, was usually used to describe the resonance frequencies of system. Figure 2 reveals the rough natural frequencies of the structure in 0.85, 2.3, 3.6, 4.8, 5.7, and 6.2 Hz, but the sixth modal is not very obvious.

The modal assurance criterion (MAC) proposed by Allemang and Brown[21] was used to check agreement between the identified mode shapes and the theoretical mode shapes

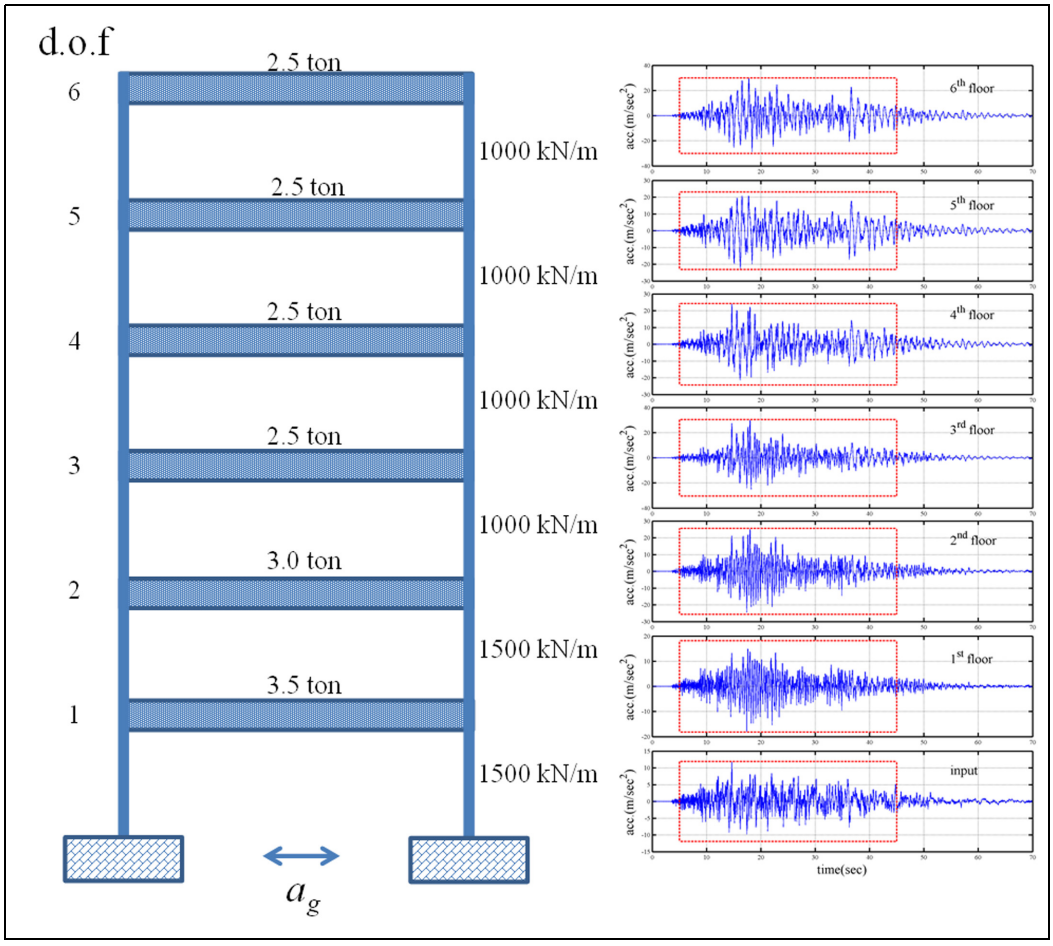

Figure 1. Schematic representation of a six-story frame and its simulation responses.

Table 1. Theoretical modal parameters of the six-story frame.

Mode	First	Second	Third	Fourth	Fifth	Sixth
f_n(Hz)	0.846	2.310	3.576	4.831	5.745	6.209
ξ(%)	5.00	5.00	5.00	5.00	5.00	5.00
Mode shapes	1.000	−0.951	−0.838	0.672	−0.443	−0.221
	0.929	−0.450	0.220	−0.877	1.000	0.619
	0.793	0.288	1.000	−0.406	−0.815	−0.896
	0.601	0.874	0.518	1.000	0.025	1.000
	0.367	1.000	−0.618	0.103	0.783	−0.909
	0.190	0.663	−0.751	−0.685	−0.753	0.586

$$\mathrm{MAC}\left(\boldsymbol{\varphi}_{k,i}, \boldsymbol{\varphi}_{k,a}\right) = \frac{\left|\boldsymbol{\varphi}_{k,i}^{\mathrm{T}}\boldsymbol{\varphi}_{k,a}\right|^2}{\boldsymbol{\varphi}_{k,i}^{\mathrm{T}}\boldsymbol{\varphi}_{k,i}\boldsymbol{\varphi}_{k,a}^{\mathrm{T}}\boldsymbol{\varphi}_{k,a}} \tag{24}$$

where $\boldsymbol{\varphi}_{k,i}$ and $\boldsymbol{\varphi}_{k,a}$ are the identified ith mode shape and the corresponding analytical mode shape, respectively. The MAC values move in the range of [0,1]. The MAC values are close to one, which indicates that the two mode shapes are similar. The MAC values are close to zero, which indicates that the two mode shapes are orthogonal to each other.

In the numerical example, the "accurate" results are should be defined as follows: the relative errors between the identified frequencies and the theoretical frequencies are within 2%, the relative errors between the identified damping ratio and the theoretical damping ratio are within 20%, and the MAC values exceed 0.95.

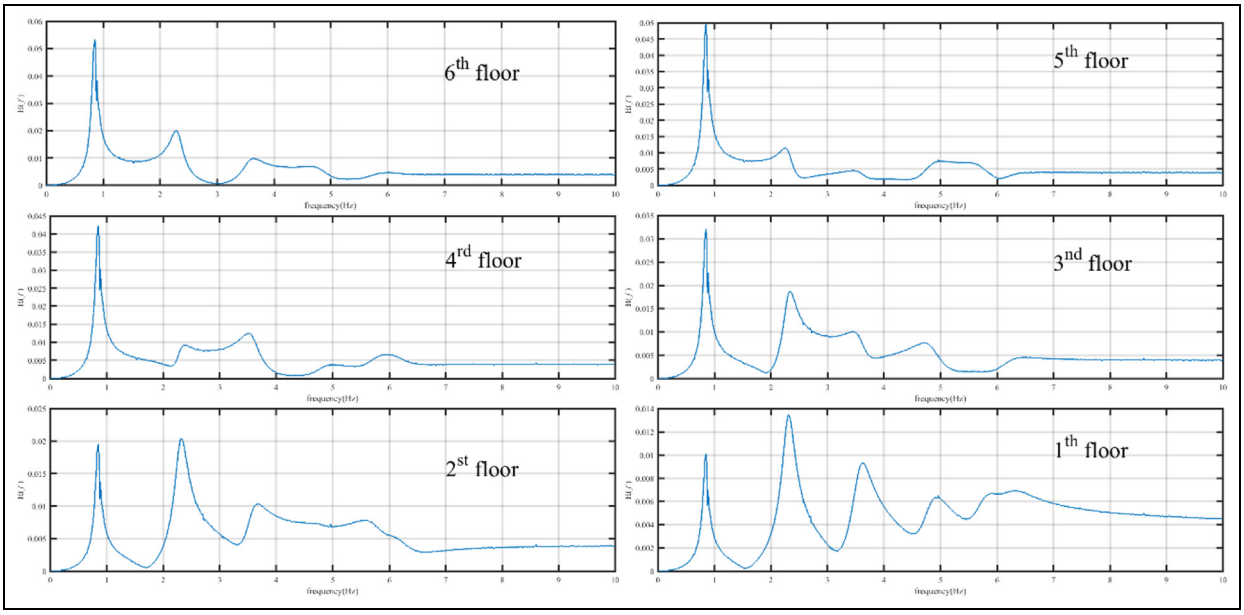

Figure 2. The frequency response function of a six-story frame.

Effects of noise

Corrupted noise always exists in the measured responses. To challenge this situation in the numerical process, the simulated responses and input excitation were randomly added by 10% variance of the NSR of noise.

The processing of noisy responses reveals the difficulty of obtaining accurate results for each mode at $s < 10$. When NSR = 5%, the first to fourth modes attained accurate damping results at $s > 35$; the fifth mode attained accurate damping result at $s > 45$; and the sixth mode could not obtain accurate damping result for $s < 50$. Figure 3(a) describes the stabilization diagrams of the identified results obtained from the noisy responses without filter.

In the Morlet wavelet domain, the interested frequency bands are retained. The continuous wavelet transform typically performs a frequency filter effect. Figure 3(b) illustrates the stabilization diagrams of the identified results in the case of processing noisy data with Morlet wavelet de-noising. The identified results via a filter theorem are as follows: the first to fourth modes attained accurate damping results at $s > 15$, the fifth mode attained accurate damping result at $s > 18$, and the sixth mode could not obtain an accurate damping ratio for $s < 22$. Figure 3 reveals the more accurate natural frequencies of the structure than the frequency response function in 0.846, 2.310, 3.575, 4.829, 5.747, and 6.207 Hz, including the highest modal. Some interested frequency ranges were kept, which was useful for obtaining accurate damping results.

As mentioned previously, the existing error in the identified higher modal was larger than the errors obtained for the other identified modals because the de-noising procedure removes certain parts' signal energy. Figure 3 reveals that the de-noising procedure significantly altered the identified fifth and sixth mode shapes, and its MAC values are less than 0.98. Figure 4 shows that the MAC values after the Gram–Schmidt process and modified Gram–Schmidt process are applied to the identified mode shapes using various values of s. The identified fifth and sixth mode shapes are corrected and its MAC values exceed 0.99 at $(I, J) > 10$. The identified mode shapes were corrected by classical Gram–Schmidt algorithm compared a bit poorly with that was corrected by modified Gram–Schmidt algorithm, but not obvious. The identified mode shapes are independent and like orthogonal set; for this reason, similar results can be obtained by these two algorithms.

Constructing a stiffness matrix

For the assumption of a given mass matrix, combined with the identified natural frequencies and corrected mode shapes, the stiffness matrix of a structure can be determined by equation (18). Considering the original shear building model as "frame A," "frame B" was created by reducing the local stiffness of the first story and third story of "frame A" to 800 and 1200 kN/m, respectively. Because both models are shear building, the theoretical stiffness matrix of both models is a tri-diagonal matrix, and one will focus on the relative errors of tri-diagonal elements in the following numerical study.

Table 2 lists the relative errors of the calculated stiffness matrix using equation (18). The modal parameters

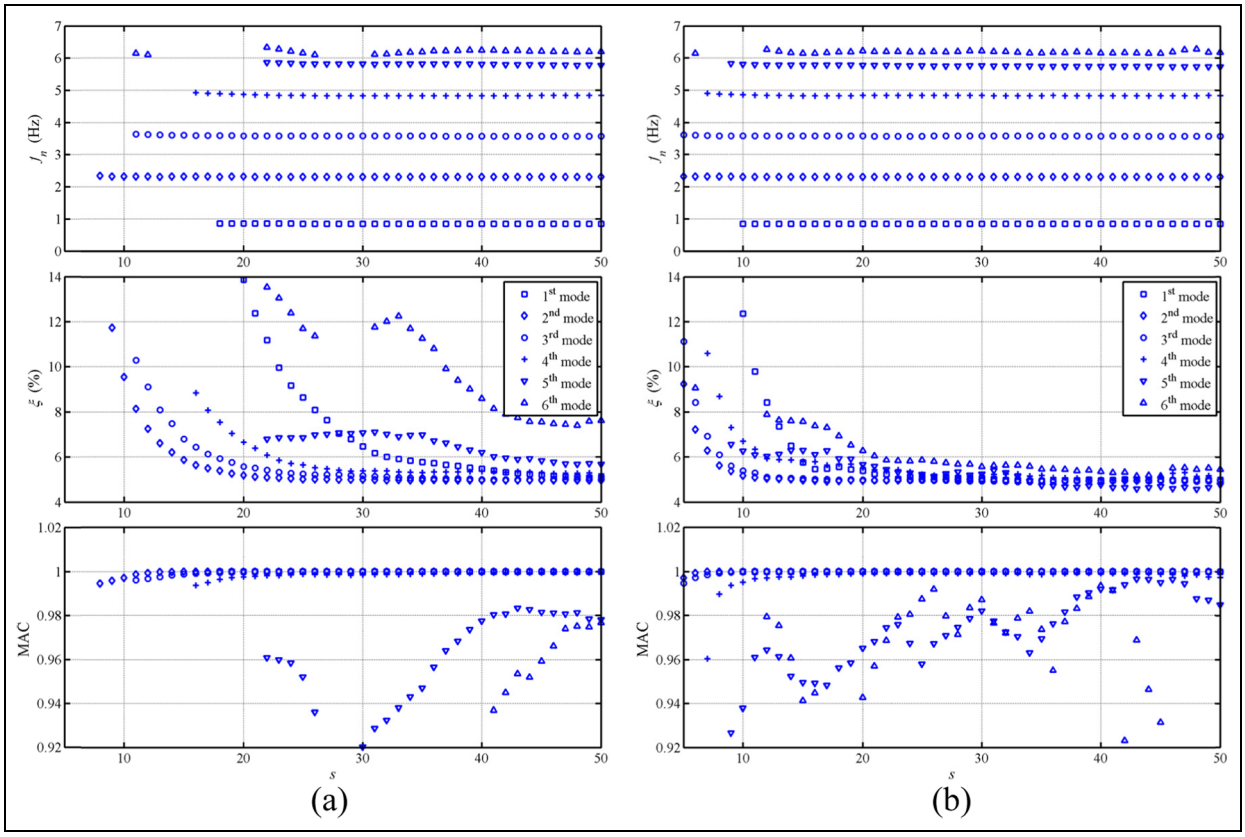

Figure 3. Stabilization diagrams of the identified results: (a) without a filter and (b) after de-noising by Morlet wavelet.

Table 2. Estimated stiffness matrix and its relative error (without correcting the identified mode shapes).

	Stiffness matrix					
Frame A	**1005.679 (0.568%)**	**−1009.295 (0.929%)**	−1.707	−26.118	−5.944	−1.221
	−1009.295 (0.929%)	**2018.604 (0.930%)**	**−984.881 (1.512%)**	51.134	25.516	1.408
	−1.707	**−984.881 (1.512%)**	**1922.019 (3.899%)**	**−997.626 (0.237%)**	−48.759	5.081
	−26.118	51.134	**−997.626 (0.237%)**	**1978.508 (1.075%)**	**−921.725 (7.827%)**	−90.224
	−5.944	25.516	−48.759	**−921.725 (7.827%)**	**2603.219 (4.129%)**	**−1520.698 (1.380%)**
	−1.221	1.408	5.081	−90.224	**−1520.698 (1.380%)**	**2924.168 (2.528%)**
Frame B	**1032.500 (3.250%)**	**−1070.332 (7.033%)**	52.096	−77.855	−5.960	−70.882
	−1070.332 (7.033%)	**2090.303 (4.515%)**	**−997.328 (0.267%)**	67.212	41.677	165.054
	52.096	**−997.328 (0.267%)**	**1915.541 (4.223%)**	**−996.853 (0.315%)**	−157.634	−71.003
	−77.855	67.212	**−996.853 (0.315%)**	**1899.878 (5.549%)**	**−778.033 (2.746%)**	158.965
	−5.960	41.677	−157.634	**−778.033 (2.746%)**	**2170.846 (5.615%)**	**−1511.971 (0.798%)**
	−70.882	165.054	−71.003	158.965	**−1511.971 (0.798%)**	**2806.405 (3.941%)**

Note: Because of shear building, the bold values are represented to results focused on tri-diagonal elements of matrix.

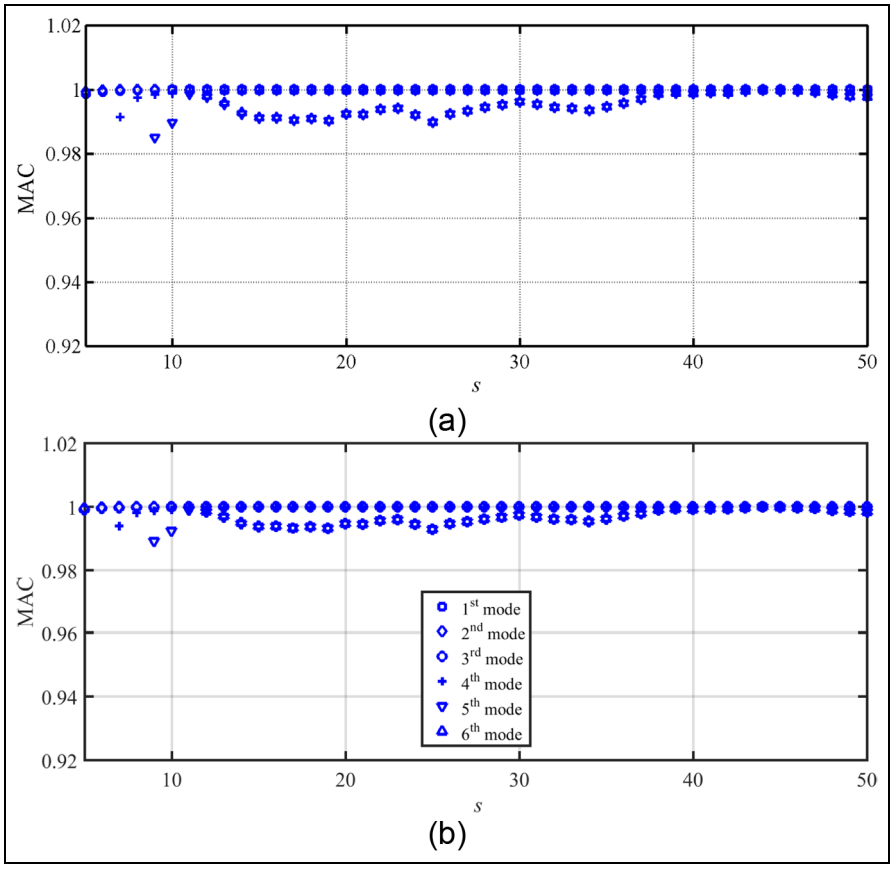

Figure 4. Stabilization diagrams of the identified mode shapes: (a) corrected by the Gram–Schmidt process and (b) corrected by the modified Gram–Schmidt process.

Table 3. The estimated stiffness matrix and its relative error (identified mode shapes corrected by Gram–Schmidt process).

	Stiffness matrix					
Frame A	**993.009 (0.699%)**	**−987.187 (1.281%)**	−10.334	4.971	−8.821	10.730
	−987.187 (1.281%)	**1975.543 (1.223%)**	**−973.735 (2.626%)**	−20.714	25.241	−25.385
	−10.334	**−973.735 (2.626%)**	**1961.160 (1.942%)**	**−962.204 (3.780%)**	−38.300	32.145
	4.971	−20.714	**−962.204 (3.780%)**	**1959.807 (2.010%)**	**−975.316 (2.468%)**	−11.932
	−8.821	25.241	−38.300	**−975.316 (2.468%)**	**2523.684 (0.947%)**	**−1543.922 (2.928%)**
	10.730	−25.385	32.145	−11.932	**−1543.922 (2.928%)**	**3066.367 (2.212%)**
Frame B	**1009.182 (0.918%)**	**−1017.580 (1.758%)**	17.394	−5.771	7.541	−4.765
	−1017.580 (1.758%)	**2035.744 (1.787%)**	**−1039.315 (3.932%)**	20.523	−22.101	16.429
	17.394	**−1039.315 (3.932%)**	**2035.590 (1.780%)**	**−1022.276 (2.228%)**	21.317	−19.013
	−5.771	20.523	**−1022.276 (2.228%)**	**1821.097 (1.172%)**	**−817.916 (2.239%)**	14.198
	7.541	−22.101	21.317	**−817.916 (2.239%)**	**2312.837 (0.558%)**	**−1502.725 (0.182%)**
	−4.765	16.429	−19.013	14.198	**−1502.725 (0.182%)**	**2692.001 (0.296%)**

Note: Because of shear building, the bold values are represented to results focused on tri-diagonal elements of matrix.

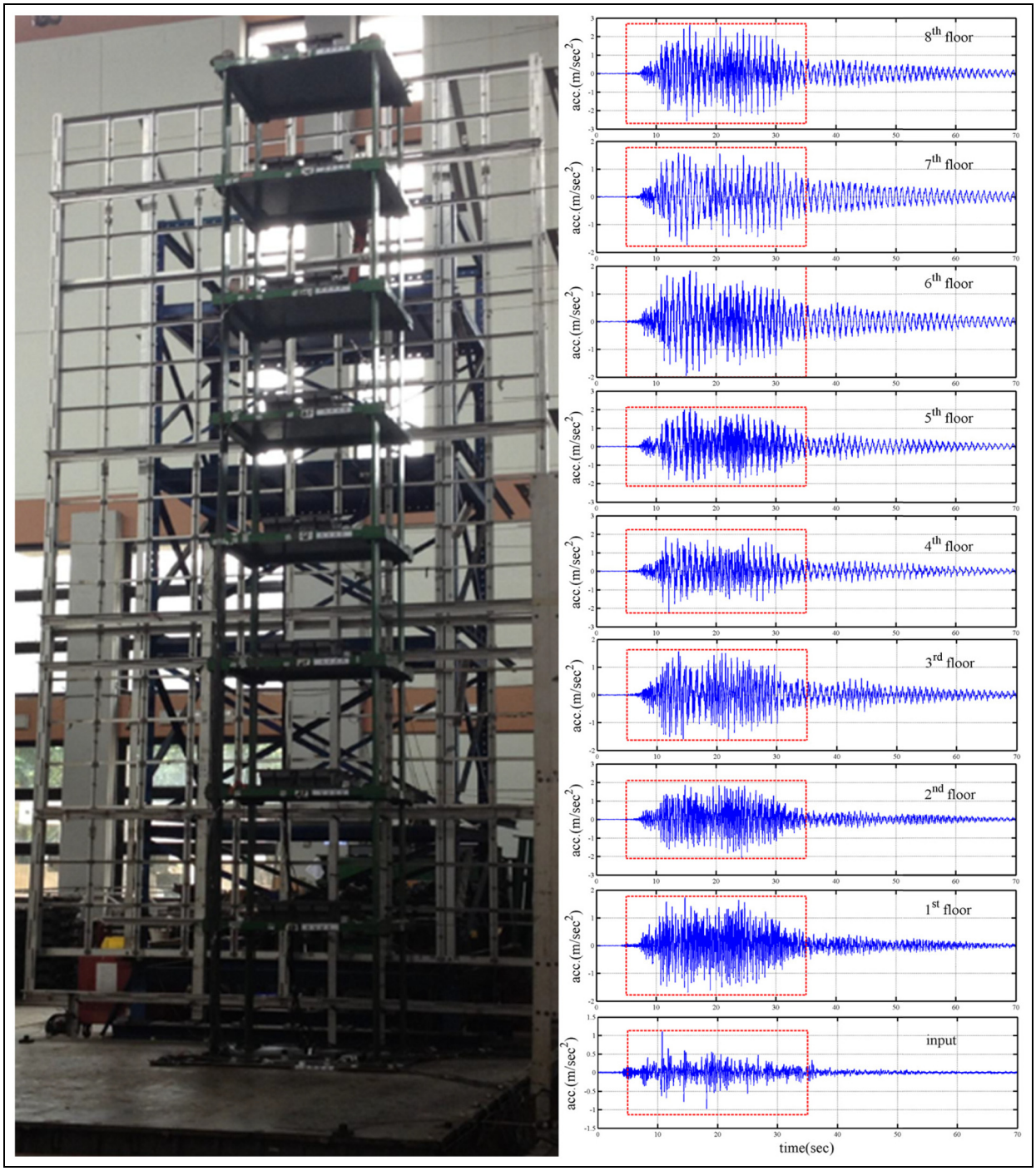

Figure 5. Photograph and time history of an eight-story frame.

that would be used in equation (18) were identified from the noisy simulation dynamic responses in the Morlet wavelet domain. For the "frame A" and "frame B," the maximum relative errors are 7.827% and 7.033%, respectively. Evaluating whether the variant of the local stiffness is less than 5% is difficult based on the identified modal parameters. For this reason, the difference of local stiffness between "frame A" and "frame B" which were created without a mode shape correction procedure is not very clear.

The proposed procedure is used to create the stiffness of "frame A" and the stiffness of "frame B" from the noisy dynamic responses. Table 3 also lists the relative errors of the calculated stiffness matrix using the Gram–Schmidt process and equation (18). The modal parameter that is employed in the Gram–Schmidt

Table 4. Identified natural frequencies and damping ratios of both the "standard" and "cutoff" frames.

Frame	Mode	First	Second	Third	Fourth	Fifth	Sixth	Seventh	Eighth
Standard	f_n(Hz)	1.052	3.112	5.179	7.123	8.921	10.469	11.725	12.512
	ξ(%)	0.636	0.251	0.213	0.176	0.175	0.172	0.179	0.195
Cutoff	f_n(Hz)	1.007	3.057	5.089	6.981	8.825	10.407	11.572	12.441
	ξ(%)	0.693	0.379	0.301	0.287	0.219	0.216	0.185	0.170

Figure 6. A photograph of a steel plate with cutoff.

process and equation (18) was also identified from the noisy simulation dynamic responses in the Morlet wavelet domain. For "frame A" and "frame B," the maximum relative errors are 3.780% and 3.932%, respectively. Evaluating whether the variant of the local stiffness exceeds 5% is easy based on the identified modal parameters. Therefore, the difference in local stiffness between "frame A" and "frame B," which were created by the proposed procedure, is very clear.

Application to a shake table test

To extend the applicability of the proposed approach when using practical measurements, the responses of two eight-story steel frame were measured in shaking table tests. The tests were performed in the laboratory of the National Center for Research on Earthquake Engineering in Taipei City, Taiwan (Figure 5). The first frame, which is structurally regular, was denoted as "standard." The length, width, and height of the frame were 1.8, 1.2, and 8.5 m (Figure 5), respectively. Lead plates were piled on each floor such that the total mass of the steel frame was approximately 4.519 tons. The second frame, which is structurally irregular with respect to stiffness and denoted as "cutoff" was identical to "standard," with the exception that the columns of the first and third stories were constructed of steel plates with cutoff, as shown in Figure 6, and others are constructed with intact steel plates.

Both frames were subjected to base excitations of the 1999 Chi-Chi earthquake, which occurred on 21 September 21 1999 in Chi-Chi, Nantou County, Taiwan, with a 100 gal (1 m/s^2) reduced level. Data were recorded at a sampling rate of 200 Hz. The acceleration responses of the base and all floors at $t = 5$–35 s were employed in the evaluation of modal parameters of the frame. Figure 5 displayed the base excitations and acceleration responses of all floors in the long-span direction of the "standard" frame, which was subjected to a 100 gal loading of the 1999 Chi-Chi earthquake.

Table 4 summarizes the identified modal parameters of both frames, and Figure 7 shows the identified mode shapes that were corrected by the Gram–Schmidt process. Figure 6 implies that the columns of the first and third stories, which were constructed by steel plates with cutoff, did not significantly alter the mode shapes. As expectation, the identified frequencies of the "standard" frame are slightly larger than the identified frequencies "cutoff" frame. Even in the higher modes, the identified modal damping ratios for different frames were smaller than 2%. A 2% of modal damping is typically adopted in the dynamic analysis of a steel structure in the design process.

Table 5 shows the final identified stiffness matrix of both frames. Variables $K_{(i)(i-1)}$ in the stiffness matrix represent the local stiffness of the story between the ith and $i-1$th floors. Table 6 lists the relative errors between the "standard" and the "cutoff" frames. K_{1g} in Table 6 indicates the stiffness values of the structural elements between the first floor and the ground floor, where $\sum_{i=1}^{8} K_{1i} + K_{1g} = 0$, thus, K_{1g} can be calculated based on K_{1i} ($i = 1$–8) for each frame.

For the condition when both the "standard" and the "cutoff" frames were subjected to a 100-gal Chi-Chi earthquake loading, the relative errors of the local stiffness between "standard" and "cutoff" frames are listed in Table 6. Compared with the "standard" frame, the stiffness values for the second, fourth, fifth, sixth, seventh, and eighth floors of "cutoff" frame do not

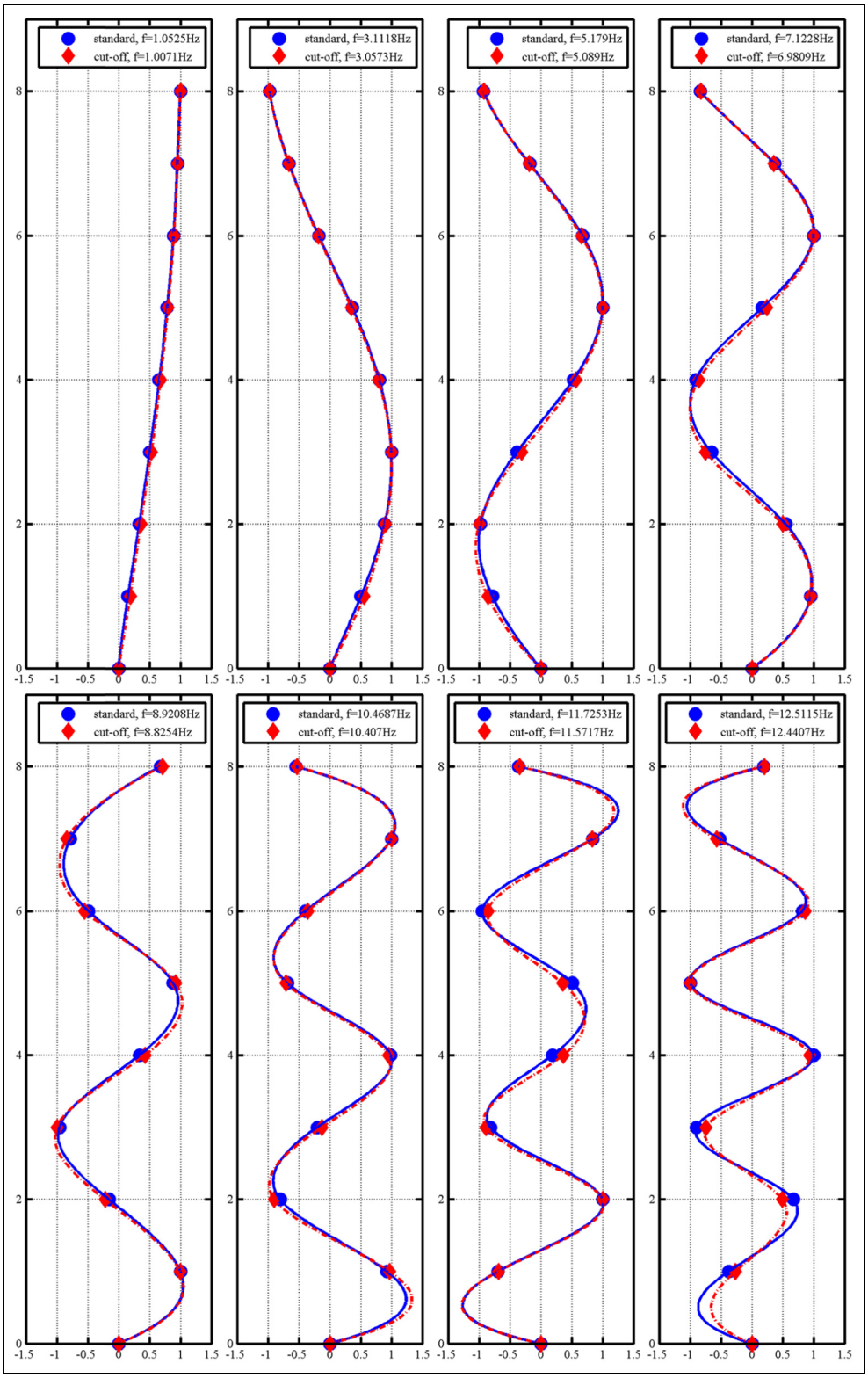

Figure 7. Identified mode shapes of both the "standard" and "cutoff" frames.

significantly change, but the stiffness values of the first and third floors decrease to 8.864% and 8.008%, respectively. These values reveal that the first and third stories of the "cutoff" frame were slightly damaged.

Table 5. Identified stiffness matrix of both the "standard" and "cutoff" frames.

	Stiffness matrix (kN/m)							
Standard	**780.2342**	**−837.836**	43.98267	−2.97081	3.552926	2.809886	0.511029	6.375347
	−837.836	**1722.024**	**−917.276**	53.47203	−5.93369	−0.04274	0.175858	2.253992
	43.98267	**−917.276**	**1722.219**	**−912.034**	56.94597	−3.09068	−0.37461	4.029386
	−2.97081	53.47203	**−912.034**	**1719.429**	**−908.316**	53.59368	−3.69292	4.611722
	3.552926	−5.93369	56.94597	**−908.316**	**1700.953**	**−901.942**	56.85761	1.024018
	2.809886	−0.04274	−3.09068	53.59368	**−901.942**	**1706.639**	**−911.585**	59.29386
	0.511029	0.175858	−0.37461	−3.69292	56.85761	**−911.585**	**1700.403**	**−896.087**
	6.375347	2.253992	4.029386	4.611722	1.024018	59.29386	**−896.087**	**1693.801**
Cutoff	**772.7837**	**−830.678**	47.54845	−2.44991	2.546618	2.228547	2.19979	1.452748
	−830.678	**1707.279**	**−917.123**	53.07994	−3.74075	0.63243	−1.50896	−0.2842
	47.54845	**−917.123**	**1723.348**	**−912.251**	55.49978	−2.69367	0.541615	−0.81442
	−2.44991	53.07994	**−912.251**	**1721.041**	**−909.132**	53.36249	−2.59622	−0.40708
	2.546618	−3.74075	55.49978	**−909.132**	**1703.184**	**−898.932**	53.25404	−4.66255
	2.228547	0.63243	−2.69367	53.36249	**−898.932**	**1635.668**	**−838.581**	50.38481
	2.19979	−1.50896	0.541615	−2.59622	53.25404	**−838.581**	**1631.751**	**−892.115**
	1.452748	−0.2842	−0.81442	−0.40708	−4.66255	50.38481	**−892.115**	**1590.285**

Note: Because of shear building, the bold values are represented to results focused on bi-diagonal elements of matrix.

Table 6. Relative errors of identified local stiffness parameters between the "standard" and "cutoff" frames.

	K_{87}	K_{76}	K_{65}	K_{54}	K_{43}	K_{32}	K_{21}	K_{1g}
Relative error (%)	0.854	0.017	0.024	0.090	0.334	**8.008**	0.443	**8.864**

Note: The bold values are to highlight the significant changes in the relative error of stiffness parameters.

Conclusion

This study presented an orthogonalization-based approach for correcting the identified mode shapes that were evaluated from structural dynamic responses in Morlet wavelet domain. The corrected mode shapes and given mass properties will be used to create an accurate stiffness matrix of a structure. This procedure is divided into the following three stages: (1) identifying the modal parameters of a structure from measured seismic responses, (2) assuming that the mass properties were given and correcting the identified mode shapes via the Gram–Schmidt process, and (3) constructing the stiffness from the identified natural frequencies and correcting the mode shapes.

In the modal identification stage, a continuous Morlet wavelet transform was applied to the measured responses; therefore, the state-variable model was reconstructed in the wavelet domain. The modal parameters of the structure were calculated from subspace approach. To reduce the numerical error of the identified mode shapes during the de-noising procedure, the mass properties and Gram–Schmidt process were used to correct the identified mode shapes. The identified natural frequencies and corrected mode shapes were employed to construct the stiffness matrix of the structure.

To validate the proposed procedure, the numerically simulated responses of a six-story shear building model subjected to earthquake input were employed in the identification process. The noise effects on the ability to precisely identify the stiffness matrix were also investigated. The proposed procedure determined stiffness parameters that were more accurate than the stiffness parameters of the procedure without mode shape correction.

The real measured data of two eight-story steel frames, with a length, width, and height of 1.8, 1.2, and 8.5 m, respectively, from a shaking table test are analyzed to demonstrate the applicability of the proposed procedure to real structures. The proposed method successfully proved that the stiffness values of these two frames differed between the first story and third story. This comprehensive procedure, which was applied to the experimental responses, demonstrates its practical applicability to a real symmetrical building.

Acknowledgements

The authors are grateful for the help provided by The Ministry of Science and Technology of the Republic of China, Taiwan. They also appreciate both the National Center for Research on Earthquake Engineering and J. J. Cloud Corp. for providing shaking table test data and communication of the measured vibration, respectively.

Declaration of conflicting interests

The author(s) declared no potential conflicts of interest with respect to the research, authorship, and/or publication of this article.

Funding

The author(s) disclosed receipt of the following financial support for the research, authorship, and/or publication of this article: This study is financially supported by The Ministry of Science and Technology of the Republic of China, Taiwan, contract no. MOST 105-2622-M-492-001-CC2.

References

1. Loh CH and Wu TS. Identification of Fei-Tsui arch dam from both ambient and seismic response data. *Soil Dyn Earthq Eng* 1996; 15: 465–483.
2. Ali MR and Okabayashi T. System identification of highway bridges from ambient vibration using subspace stochastic realization theories. *Earthq Struct* 2011; 2: 189–206.
3. Ibrahim SR and Mikulcik EC. The experimental determination of vibration parameters from time responses. *Shock Vib Bull* 1976; 46: 187–196.
4. Huang CS, Hung SL, Lin CI, et al. A wavelet-based approach to identifying structural modal parameters from seismic response and free vibration data. *Comput-Aided Civ Inf* 2005; 20: 408–423.
5. Su WC, Huang CS, Chen CH, et al. Identifying the modal parameters of structure from ambient vibration data via the stationary wavelet packet. *Comput-Aided Civ Inf* 2014; 29: 738–757.
6. Huang CS and Lin HL. Modal identification of structures from ambient vibration, free vibration, and seismic response data via a subspace approach. *Earthq Eng Struct D* 2001; 30: 1857–1878.
7. Huang CS, Chen LJ, Hung SL, et al. Combining subspace approach and short time Fourier analysis for locating structural damage storeys. *J Vibroeng* 2015; 17: 2480-2490.
8. Ruzzene M, Fasana A, Garibaldi L, et al. Natural frequencies and dampings identification using wavelet transform: application to real data. *Mech Syst Signal Pr* 1997; 11: 207–218.
9. Lardies J and Gouttebroze S. Identification of modal parameters using the wavelet transform. *Int J Mech Sci* 2002; 44: 2263–2283.
10. Le TP and Argoul P. Continuous wavelet transform for modal identification using free decay response. *J Sound Vib* 2004; 277: 73–100.
11. Huang CS and Su WC. Identification of modal parameters of a time invariant linear system by continuous wavelet transformation. *Mech Syst Signal Pr* 2007; 21: 1642–1664.
12. He J and Ewins DJ. Analytical stiffness matrix correction using measured vibration modes. *Int J Anal Exp Modal Anal* 1995; 1: 9–14.
13. He W and Ge SS. Vibration control of a flexible beam with output constraint. *IEEE T Ind Electron* 2015; 62: 5023–5030.
14. He W, Sun C and Ge SS. Top tension control of a flexible marine riser by using integral-barrier Lyapunov function. *IEEE/ASME T Mech* 2015; 20: 497–505.
15. He W, Ouyang Y and Hong J. Vibration control of a flexible robotic manipulator in the presence of input deadzone. *IEEE T Ind Electron* 2017; 13: 48–59.
16. Bjorck A. *Numerical methods for least squares problems*. Philadelphia, PA: SIAM, 1998.
17. Stewart GW. *Matrix algorithms volume I: basic decompositions*. Philadelphia, PA: SIAM, 1998.
18. Bjorck A. Solving linear least squares problems by Gram-Schmidt orthogonalization. *BIT* 1967; 7: 1–21.
19. Wilkinson JH. Modern error analysis. *SIAM Rev* 1971; 13: 548–569.
20. Tedesco JW, McDougal WG and Ross CA. *Structural dynamics: theory and applications*. Menlo Park, CA: Addison-Wesley, 1999.
21. Allemang RL and Brown DL. A correlation coefficient for modal vector analysis. In: *Proceedings of the 1st international modal analysis conference* & exhibit, Orlando, FL, 8–10 November 1982, pp. 110–116. Union College.